1

2 **Warm Winter, Thin Ice?**

3 Julienne Stroeve[1,2], David Schroder[3], Michel Tsamados[1], Daniel Feltham[3]

4

5 [1]Centre for Polar Observation and Modelling, Earth Sciences, University College London,
6 London, UK
7 [2]National Snow and Ice Data Center, University of Colorado, Boulder, CO, USA
8 [3]Centre for Polar Observation and Modelling, Department of Meteorology, University of
9 Reading, Reading, UK

10

11 **Abstract**

12 Winter 2016/2017 saw record warmth over the Arctic Ocean, leading to the least amount of
13 freezing degree days north of 70°N since at least 1979. The impact of this warmth was
14 evaluated using model simulations from the Los Alamos sea-ice model (CICE) and CryoSat-
15 2 thickness estimates from three different data providers. While CICE simulations show a
16 broad region of anomalously thin ice in April 2017 relative to the 2011-2017 mean, analysis
17 of three CryoSat-2 products show more limited regions with thin ice and do not always agree
18 with each other, both in magnitude and direction of thickness anomalies. CICE is further used
19 to diagnose feedback processes driving the observed anomalies, showing 11-13 cm reduced
20 thermodynamic ice growth over the Arctic domain used in this study compared to the 2011-
21 2017 mean, and dynamical contributions of +1 to +4 cm. Finally, CICE model simulations
22 from 1985-2017 indicate the negative feedback relationship between ice growth and winter
23 air temperatures may be starting to weaken, showing decreased winter ice growth since 2012
24 as winter air temperatures have increased and the freeze-up has been further delayed.

25

26 **Introduction**

27   It is well known that Arctic air temperatures are rising faster than the global average [e.g.
28 *Bekryaev et al*., 2010; *Serreze and Barry*, 2011]. The thinning and shrinking of the summer
29 sea ice cover have played a role in this amplified warming, which is most prominent during
30 the autumn and winter months as the heat gained by the ocean mixed layer during ice-free
31 summer periods is released back to the atmosphere during ice formation [e.g. *Serreze et al*.,
32 2009; *Screen and Simmonds*, 2010]. However, Arctic amplification has been found in climate
33 models without changes in the sea ice cover [*Pithan and Mauritsen*, 2014]. Increased latent
34 energy transport [*Graversen and Burtu*, 2016], the lapse rate feedback [*Pithan and*
35 *Mauritsen*, 2014; *Graversen*, 2006] and changes in ocean circulation [*Polyakov et al*., 2005]
36 have also contributed. Furthermore, cyclones are effective means of bringing warm and moist
37 air into the Arctic during winter [e.g. *Boisvert et al*., 2016].
38   Winter 2015/2016 was previously reported as the warmest Arctic winter recorded since
39 records began in 1950 [*Cullather et al*., 2016]. Warming was Arctic-wide, with temperature
40 anomalies reaching +5°C [*Overland and Wang*, 2016] and temperatures near the North Pole
41 hitting 0°C [*Boisvert et al*., 2016]. Part of the unusual warming was linked to a strong cyclone
42 that entered the Arctic in December 2015 [*Boisvert et al*., 2016], resulting in reduced
43 thermodynamic ice growth and thinning within the Kara and Barents seas [*Ricker et al.*,
44 2017; *Boisvert et al*., 2016]. This was one of several cyclones to enter the Arctic that winter
45 as a result of a split tropospheric vortex that brought warm and moist air from the Atlantic
46 Ocean towards the pole [*Overland and Wang*, 2016]. Winter 2016/2017 once again saw
47 temperatures near the North Pole reach 0°C in December 2016 and February 2017 [*Graham*
48 *et al*., 2017]. These warming events were similarly associated with large storms entering the
49 Arctic [*Cohen et al*., 2017]. It has been suggested that the recent warm winters represent a

The Cryosphere
Discussions
Open Access
EGU

50 trend towards increased duration and intensity of winter warming events within the central
51 Arctic [*Graham et al*., 2017].
52   In general, warm winters, combined with increased ocean mixed layer temperatures from
53 summer sea ice loss, delay freeze-up, impacting the length of the ice growth season and the
54 period for snow accumulation on the sea ice. *Stroeve et al*. [2014] previously evaluated
55 changes in the melt onset and freeze-up, showing large delays in freeze-up within the
56 Chukchi, East Siberian, Laptev and Barents seas, with delays increasing on the order of +10
57 days per decade. Later freeze-up has a non-trivial influence on basin-wide sea ice thickness:
58 ice grows thermodynamically faster for thin ice than for thick ice [*Bitz and Roe*, 2004]. More
59 subtle effects involving the timing of ice growth relative to major snow precipitation events
60 in fall have been shown to also control the growth rate of sea ice thickness; ice grows faster
61 for a thinner snow pack [*Merkouriadi et al*., 2017]. Nevertheless, the maximum winter sea
62 ice extent in 2017 set a new record low for the 3rd year in a row. Have the recent warm
63 winters played a role in these record low winter maxima by reducing winter ice formation?
64   *Ricker et al.* [2017a] previously evaluated the impact of the 2015/2016 warm winter on
65 ice growth using sea ice thickness derived from blending CryoSat-2 (CS2) radar altimetry
66 with those from Soil Moisture and Ocean Salinity (SMOS) radiometry [*Ricker et al*., 2017b].
67 They found anomalous freezing degree days (FDDs) between November 2015 and March
68 2016 within the Barents Sea of 1000 degree days coincided with a thinning of approximately
69 10 cm in March compared to the 6-year mean. While near-surface air temperatures largely
70 control thermodynamic ice growth, other processes also impact ice growth, including ocean
71 circulation, sensible and latent heat exchanges. Furthermore, winter ice thickness is not only
72 a result of thermodynamic ice growth, but rather the combined effects of thermodynamic and
73 dynamic processes. A thinner ice cover is more prone to ridging and rafting, as well as ice
74 divergence, leading to new ice formation within leads/cracks within the ice pack. This
75 however was not evaluated by *Ricker et al*. [2017a].
76   In this study we evaluate the impact of the 2016/2017 anomalously warm winter on
77 Arctic sea ice thickness using the Los Alamos sea-ice model (CICE) [*Hunke et al.,* 2015] and
78 satellite-derived CS2 thickness data from three different sources: Centre for Polar
79 Observation and Modeling (CPOM) [*Tilling et al*., 2017], Alfred Wegener Institute (AWI)
80 [*Hendricks et al*., 2016], and NASA [*Kurtz and Harbeck*, 2017]. CICE is initialized with
81 CPOM CS2 sub-grid scale ice thickness distribution (ITD) fields in November and run
82 forward with NCEP Reanalysis-2 (NCEP2) atmospheric reanalysis data [*Kanamitsu et al*.,
83 2002, updated 2017]. The model run is subsequently compared over the winter growth season
84 to CS2 thickness from the three different data providers and contributions of thermodynamics
85 vs. dynamics to the thickness anomalies are evaluated. While the focus is on the 2016/2017
86 ice growth season, a secondary aim is to compare existing CS2 products to inform the
87 community on uncertainties in these estimates and inform on model limitations. Thus, results
88 are also presented for other years during the CS2 time-period for comparison. To our
89 knowledge, this is the first study to compare different CS2 data products over the lifetime of
90 the mission.
91
92 **Methods**
93 *Ice Thickness Distribution (ITD) from Cryosat-2*
94   The CryoSat-2 radar altimetry mission was launched April 2010, providing estimates of
95 ice thickness during the ice growth season. CS2 provides freeboard estimates, or the height of
96 the ice surface above the local sea surface, which when combined with information on snow
97 depth, snow density and ice density can be converted to ice thickness assuming hydrostatic
98 equilibrium [e.g. *Laxon et al*., 2013]. Here we evaluate ice thickness fields provided by three
99 different data providers in order to assess robustness of the observed thickness anomalies.

100 Thickness is retrieved from ice freeboard by processing CS2 Level 1B data, with a footprint
101 of 300m by 1700m, and assuming snow density and snow depth from the *Warren et al.*
102 [1999] climatology (hereafter *W99*), modified for the distribution of multiyear versus first-
103 year ice (i.e. snow depth is halved over first-year ice) [see *Laxon et al.*, 2013 and *Tilling et*
104 *al.*, 2017 for data processing details].
105   While the three data providers rely on *W99* for snow depth and density, each institution
106 processes the radar returns differently. In general, the range to the main scattering horizon of
107 the radar return is obtained using a retracker algorithm. This can be based on a threshold [e.g
108 *Laxon et al.*, 2013; *Ricker et al.*, 2014; *Hendricks et al.*, 2016], or a physical retracker [*Kurtz*
109 *et al.*, 2014]. While the CPOM and AWI products use a leading edge 50% threshold
110 retracker, *Kurtz and Harbeck* [2017] rely on a physical model to best fit each CryoSat-2
111 waveform. This will lead to ice thickness differences based on different thresholds applied:
112 *Kurtz et al.* [2014] found a 12 cm mean difference between using a 50% threshold and a
113 waveform fitting method.
114   We note that several factors contribute to CS2-derived sea ice thickness uncertainties,
115 including the assumption that the radar return is from the snow/ice interface [*Willat et al.*,
116 2011], snow depth departures from climatology and the use of fixed snow and ice densities.
117 In this study we initialize the CICE model simulations described below with the CPOM sea
118 ice thickness fields. Accuracy of the CPOM product has been evaluated in several studies,
119 suggesting mean biases between thickness observations in 2011 and 2012 of 6.6 cm when
120 compared with airborne EM data [*Laxon et al.*, 2013; *Tilling et al.*, 2015]. For April 2017, the
121 CPOM near-real-time product [*Tilling et al.*, 2016] was used in place of the archived product,
122 with a mean thickness bias of 0.9 cm between these products.
123   In this study, individual thickness point measurements are binned into 5 CICE thickness
124 categories (1: < 0.6m, 2: 0.6-1.4m, 3: 1.4-2.6m, 4: 2.6-3.6m, 5: > 3.6m) on a rectangular
125 50km grid for each month. The mean area fraction and mean thickness is derived for each
126 thickness category and these values are interpolated on the tripolar 1 degree CICE grid
127 (~40km grid resolution). Grid points with less than 100 individual measurements and a mean
128 SIT < 0.5 m are not included. For November, this effectively limits the area of the Arctic to
129 the region shown in Figure 1(c). Negative thickness values that are retained in the CS2
130 processing to prevent statistical positive bias of the thinner ice are added to category 1. The
131 novel approach of initializing the CICE model with the full ITD rather than the mean sea ice
132 thickness provides an additional control on the repartition of the ice among different
133 thickness categories. This in turn allows a more accurate representation of ice growth and ice
134 melt processes [*Tsamados et al.*, 2015] compared to initializing with the mean grid-cell SIT
135 and deriving the fractions for each ice category assuming a parabolic distribution. Ice growth
136 and melt strongly depend on SIT: using a real distribution can have a big impact, especially
137 for thin ice.

138 *CICE Simulations*
139   CICE is a dynamic-thermodynamic sea-ice model designed for inclusion within a global
140 climate model. The advantages of using CICE for this study is that we can more readily
141 separate thickness anomalies into their thermodynamic and dynamical contributions, examine
142 inter-annual variability and perform longer simulations. For this study, we performed two
143 different CICE simulations. The first is a multiyear simulation from 1985 to 2017 (referred to
144 as CICE-free). The second is a stand-alone sea-ice simulation for the pan-Arctic region
145 starting in mid-November and running until the end of April of the following year for the last
146 7 winter periods from 2010/2011 to 2016/2017. This results in seven 1-year long simulations
147 (referred to as CICE-ini), in which the initial thickness and concentration for each of the 5 ice
148 categories is updated from the CS2 ITD using the CPOM CS2 November thickness fields.

149   For grid points without CS2 data, and for all other variables (e.g. temperature profiles, snow
150   volume), results from the free CICE simulation with the same configuration started in 1985
151   are applied. In this way, CICE simulations cover the pan-Arctic region, but in regions where
152   no CS2 are available, we restart SIT values from the free CICE model run. While this
153   approach would be problematic in a coupled model, in a stand-alone sea ice simulation the
154   model adjustment to the new conditions is smooth and the impact of using the vertical
155   temperature profile from the free simulation only affects sea ice thickness on the order of
156   millimeters. While snow accumulation can depart strongly from the *W99* climatology for
157   individual years, we make the assumption that the deviation of the mean *annual* cycle of
158   snow depth over the last 7 years from the *W99* climatology is small. Thus, we assume mean
159   winter ice growth to be determined accurately from CS2, and tuned CICE-ini accordingly to
160   match the observed CS2 mean winter ice growth from the CPOM product in the central
161   Arctic [**Figure 1**]. The excellent agreement for both CICE-ini and CICE-free with CS2
162   increases the confidence of our model results. Our approach therefore allows us to study
163   inter-annual variability from 2 model configurations with different sources of errors, in
164   addition to the 3 CS2-based products.
165   For both CICE simulations, NCEP-2 provides the atmospheric forcing. We use NCEP-2
166   2m air temperatures because they have been shown to be more realistic for the Arctic Ocean
167   than those from ERA-Interim [*Jakobshavn et al*., 2012]. The setup is the same as described *in*
168   *Schröder et al.* [2014] including a simple ocean-mixed layer model, a prognostic melt pond
169   model [*Flocco et al*., 2012] and an elastic anisotropic-plastic rheology [*Tsamados et al*.,
170   2013], with the following improvements: we apply an updated CICE version 5.1.2 with
171   variable atmospheric and oceanic form drag parameterization [*Tsamados et al*. 2014], we
172   increase the thermal conductivity of fresh ice from 2.03 W/m/k to 2.63 W/m/K, snow from
173   0.3 W/m/K to 0.5 W/m/K and the emissivity of snow and ice from 0.95 to 0.976. While the
174   default conductivity values are at the lower end of the observed range, the new values are at
175   the upper end and have been applied in previous climate simulations [e.g *Rae et al*., 2014].
176   Below, all CS2-derived sea ice thickness anomalies are computed relative to the CS2
177   time-period: November anomalies are relative to 2010-2016, and for April they are relative to
178   2011-2017. Results for November and April are only shown for all grid cells which have a
179   minimum thickness of 50 cm and a minimum of 100 individual measurements for each of the
180   seven years. For the month of November, this corresponds to all colored area shown in Figure
181   1(c). For April, this region represents the area in red shown in Figure 1(d). The larger region
182   shown in Figure 1(d) also corresponds to the region over which the amount of
183   thermodynamic ice growth and dynamical ice growth between November and April are
184   assessed from the CICE simulations. Further note that area-averaged values for November
185   and April are only given for regions shown in Figure 1(c) and Figure 1(d), respectively.
186
187   ## Results
188   ### *Air temperature and freezing anomalies*
189   The growing season air temperatures anomalies (i.e. mid-November 2016 to mid-April
190   2017 relative to 1981-2010) were positive throughout the Arctic, leading to large reductions
191   in the number of FDDs, computed as the cumulative daily 2 m NCEP-2 air temperatures
192   below -1.8°C, similar to *Ricker et al*. [2016]. FDDs computed this way reflect both the
193   number of days with air temperatures below freezing, and the magnitude of below freezing
194   air temperatures over the specified period. Spatially, FDD anomalies show widespread
195   reductions over most of the Arctic Ocean, with the largest reductions in the Barents and Kara
196   seas, stretching across the pole towards the Beaufort and Chukchi seas [**Figure 2b**]. In
197   contrast, during winter 2015/2016, FDDs were most notably anomalous within the Barents
198   and Kara seas [**Figure 2a**], in agreement with *Ricker et al*. [2017a]. Overall, as averaged

The Cryosphere
Discussions

Open Access

199   from 70-90°N, this past winter witnessed the least amount of cumulative FDDs since at least
200   1979 [**Figure 2c**].
201   While ice forms quickly within the central Arctic once air temperatures drop below
202   freezing, this year saw large delays in freeze-up throughout the Arctic. Updating results
203   previously reported in *Stroeve et al*. [2014], freeze-up was delayed by 20 days for the Arctic
204   as a whole, with regions like the Bering, Beaufort, Chukchi, East Siberian and Kara seas
205   delayed by three to four weeks [**Figure 2d**]. Within the Barents Sea, the regionally averaged
206   freeze-up was delayed by 60 days. In recent years, the trend towards later freeze-up has
207   increased, with the Barents and Chukchi seas showing the largest trends on the order of +14
208   days per decade through 2017, followed by the Kara and East Siberian seas with delays on
209   the order of +10 to +12 days per decade. Within the Beaufort Sea, freeze-up is now
210   happening later by +9 days per decade [**Table 1**].
211
212   *November ice thickness anomalies*
213   Before analyzing how the reduced number of freezing degree days impacted winter ice
214   growth during 2016/2017, it is useful to first inter-compare the different CryoSat-2 thickness
215   estimates. We start with a comparison of November thickness from the three CS2 data sets
216   from November 2010 to 2016 [**Figure 3**].
217   It is encouraging to find that year-to-year variability in the spatial patterns of positive and
218   negative thickness anomalies are generally consistent between the three products despite
219   differences in waveform processing. The AWI and CPOM data sets are in better agreement
220   with each other than with the NASA product, which is expected as they use a similar
221   retracker. Furthermore, all three data sets show widespread thinner ice in November 2011,
222   and widespread thicker ice in November 2013. This is further supported by analysis of
223   regional mean thickness and anomalies computed over the region shown in Figure 1(c)
224   [**Table 2**]. For comparison, we also list results from the CICE-free model simulation. In
225   November 2011, the different CS2 data products are in agreement that the ice was
226   anomalously thin (-32 to -46 cm), the thinnest in the CS2 data record. Similarly, in November
227   2013, all three CS2 products show overall thicker ice on the order of +23 to +38 cm. The
228   CICE-free simulations also show anomalously thinner and thicker ice during these years, but
229   larger anomalies were simulated in 2012 and 2014.
230   While the overall pattern of years with anomalously thin or thick ice is broadly similar
231   between the three CS2 products, this is not true in 2016. Both the CPOM and AWI thickness
232   estimates suggest slightly thicker ice than average (+4 cm and +9 cm, respectively), while the
233   NASA product suggests the icepack was overall slightly thinner (-1 cm). The CICE-free run
234   is in agreement with the NASA data set for the 2016 anomaly. Turning back to **Figure 3**, we
235   find that in 2016 the CPOM data set shows +20 to +60 cm thicker ice north of the Canadian
236   Archipelago (CAA) and Greenland, -20 to -60 cm thinner ice on the Pacific side of the pole,
237   and +10 to +30 cm thicker ice north of the Laptev Sea. These spatial patterns of November
238   2016 SIT anomalies are broadly similar with those from AWI but less so with NASA.
239   However, despite similar patterns of positive and negative thickness anomalies, AWI shows
240   between +20 and +30 cm thicker ice over much of the central Arctic Ocean, and even thicker
241   ice (up to +60 cm) north of the CAA and Greenland in November 2016 than the CPOM
242   product. NASA on the other hand shows larger negative anomalies on the Pacific side of the
243   north pole of up to -70 cm and larger positive anomalies directly north of the CAA between
244   +10 and +20 cm.
245   Since we use CPOM CS2 thickness fields to initialize our CICE model runs, this
246   comparison is useful in determining whether or not the 2016 November thickness anomalies
247   are robust in other CS2 processing streams and provides a measure of CS2 sea ice thickness
248   uncertainty.

The Cryosphere
Discussions

249　However, since we do not have the AWI and NASA ITDs we cannot quantify the impact of
250　using a different thickness data set on our simulations. However, as a result of the negative
251　winter ice growth feedback (discussed below), differences due to model initialization in
252　November will be attenuated until April.
253
254　*Sea Ice growth from November to April*
255　　For a more robust analysis of winter ice growth during the record warm winter of
256　2016/2017, we now include April thickness estimates from CS2 (CPOM, AWI and NASA),
257　the free CICE simulation and the CICE simulations initialized with CPOM CS2 November
258　SIT in **Figure 4**. Corresponding values for all other years are shown in **Figure 5** (CS2) and
259　**Figure 6** (CICE). **Table 3** summarizes associated mean April thickness and anomalies since
260　2011, together with contributions from thermodynamics (ice growth) and dynamics (ice
261　transport and ridging) based on the CICE model simulations. The area for which these
262　estimates are provided corresponds to the area shown in Figure 1(d).
263　　We first note that all 5 estimates have different strengths and weaknesses: while the mean
264　annual cycle of sea ice thickness *should* be more accurate from CS2 than modeled estimates,
265　robust analysis of winter ice growth from CS2 is in part limited due to the impact of
266　climatological snow depth assumptions, which may differ from one year to the next, and
267　differences in waveform processing between CS2 data providers, which may result in
268　inconsistencies in the magnitude and direction of the observed thickness anomalies. In the
269　free CICE simulation, November sea ice thickness is less certain due to error accumulation
270　during the model run. In the initialized CICE simulation, both these error sources are reduced
271　but inherent model biases remain.
272　　Despite these limitations, all five approaches show good agreement in most years
273　regarding the direction of the thickness anomalies (i.e. positive or negative) even if they
274　disagree on absolute magnitude. For example, Arctic Ocean mean thickness anomalies are
275　negative in all 3 CS2 products for April 2013 (ranging from -3 to -25 cm), whereas in April
276　2014 and 2015 all approaches give positive mean thickness anomalies, ranging from +5 to
277　+20 cm in 2014 and +11 to +22 cm in 2015 [**Table 3**]. In some years, the CICE-free
278　simulation better matches the observed April thickness anomalies (e.g. 2013, 2015), whereas
279　in other years CICE-ini performs better (e.g. 2012, 2014). On the other hand, in 2011 and
280　2017 we find disagreement among the three CS2 data sets. In April 2011, both the CPOM
281　and NASA product have overall negative thickness anomalies for the Arctic Basin (-4 and -8
282　cm, respectively), whereas they are positive in the AWI product (+7 cm). In April 2017, both
283　the CPOM and AWI are in close agreement that the ice cover was overall thinner (-13 and -
284　12 cm, respectively), as are the CICE-free and CICE-ini simulations (negative thickness
285　anomalies of -13 cm), whereas NASA shows a weak positive anomaly (+3cm).
286　　Focusing more on April 2017, the 3 CS2 products suggest sea ice within the Chukchi and
287　East Siberian seas was on average -10 to -35 cm thinner in April 2017 compared to the 2011-
288　2017 mean **[Figure 4(top)]**. CICE simulations show more widespread thinning throughout
289　the western Arctic, including the Beaufort Sea **[Figure 4(middle and bottom)]**. In the
290　Beaufort Sea, there is general disagreement among the 3 CS2 products and the CICE
291　simulations: regional mean anomaly of -5 cm (CPOM), 0 cm (AWI), +20 cm (NASA), -25
292　cm (CICE-ini) and -30 cm (CICE-free). There is also disagreement north of the CAA, with
293　CICE-ini indicating positive thickness anomalies (up to +50 cm), whereas all 3 CS2 products
294　generally show negative thickness anomalies (up to -80 cm). In this region, the CICE-free
295　simulation also shows mostly negative thickness anomalies (-20 to -80 cm), with a small
296　positive area (up to +25 cm).
297　　While the discrepancy in this region is puzzling, the bias between the CICE-ini
298　simulations and the CS2 products in part may reflect the use of a snow climatology in the

The Cryosphere
Discussions

Open Access

299 CS2 thickness retrievals. As discussed earlier, a positive sea ice thickness anomaly was found
300 in the November 2016 CS2 thickness retrievals north of CAA and Greenland. Yet this
301 positive thickness anomaly is not preserved through April in both the CPOM and AWI CS2
302 products. **Figure 7** shows CICE simulated snow depth anomalies in November 2016 and
303 April 2017. In November, small positive snow depth anomalies occur throughout the Arctic,
304 especially north of the Queen Elizabeth Islands where the anomaly locally increases to 20
305 cm. By April, the anomalies cover a broader region and increase in magnitude. A positive
306 April snow depth anomaly of 15 to 20 cm relative to *W99* would result in an underestimation
307 of the CS2-retrieved April ice thickness (SIT) by 79 to 106 cm using the following equation
308 [*Armitage et al.*, 2015]:
309
310
$$SIT = \frac{\rho_{snow} H_{snow} + \rho_{water} F_i}{(\rho_{water} - \rho_{ice})}$$

311
312 where we choose snow density (ρ_{snow}) of 320 kg/m^3 [*Warren et al.*, 1999], ice density (ρ_{ice}) of
313 915 kg/m^3, water density of (ρ_{water}) 1024 kg/m^3. For a radar penetrating to the ice-snow
314 interface and accounting for the reduced propagation of the speed of light through the snow
315 cover (2.4 10^8 m/s [Tilling et al., 2017]) the ice freeboard (F_i) as a function of the radar
316 freeboard (F_b) is $F_i = F_b + 0.25H_{snow}$. CICE-ini, which relies on the CPOM CS2 November
317 thickness, maintains this positive thickness anomaly through April despite reduced
318 thermodynamic ice growth. The CICE-free simulation on the other hand started with negative
319 thickness anomalies in November within this region, and maintains them through April.
320   One advantage of using CICE, is that we can more readily diagnose thermodynamic vs.
321 dynamical contributions to the observed thickness anomalies. CICE simulations suggest the
322 overall thinner ice in April 2017 is largely attributed to reduced thermodynamic ice growth.
323 One would expect thermodynamic ice growth to be reduced in regions of enhanced snow
324 depth and thicker November ice. Spatially, the largest reductions in thermodynamic ice
325 growth during winter 2016/2017 occurred within the Chukchi Sea and north of the CAA and
326 extending through the northern Beaufort Sea (on the order of -40 cm). These regions have
327 very different explanations for reduced thermodynamic ice growth. Ice formed a month later
328 than the 1981-2010 mean within the Chukchi Sea, reducing the number of days over which
329 the ice could grow. In contrast, north of the CAA, winter ice growth was reduced in a region
330 that showed positive November thickness anomalies, illustrating the strong dependence of
331 thermodynamic ice growth on initial ice thickness. This region also had anomalously positive
332 snow depths that extended through the northern Beaufort Sea, in agreement with extended
333 regions of reduced thermodynamic ice growth.
334   While the CICE simulations show reduced thermodynamic ice growth for most of the
335 Arctic over winter 2016/2017, ice growth was enhanced directly north of Utqiaġvik, Alaska
336 (formerly Barrow). However, this enhanced ice growth was offset by ice divergence, leading
337 to overall thinner ice in the CICE simulations. In situ observations of level first-year ice
338 thickness off the coast of Utqiaġvik ranged between 1.35 and 1.40m during May
339 (http://arcus.org/sipn/sea-ice-outlook/2017/june) and appear to be in better agreement with
340 the CICE simulations, as well as the CPOM and AWI CS2 thickness estimates, while the
341 NASA CS2 product shows positive thickness anomalies in that region. Positive
342 thermodynamic ice growth anomalies are also found for a small region north of Greenland
343 and within Fram Strait, as well as within some scattered coastal regions of the Chukchi, East
344 Siberian, Laptev and Kara seas.
345   Finally, dynamical thickness changes simulated by CICE show an overall thickening of
346 the ice in winter 2016/2017 particularly within the Chukchi and Bering seas (up to 50 cm).

The Cryosphere
Discussions
Open Access
EGU

347   Anomalous ridging in this region is in agreement with observed high amounts of deformation
348   along the shore fast ice zone within the Chukchi Sea as a result of persistent west winds from
349   December to March (http://arcus.org/sipn/sea-ice-outlook/2017/june). Even larger dynamical
350   thickening was found within the Kara and northern Barents seas (up to 1.2 m) and to a lesser
351   extent over the southern and western Greenland Sea, Baffin Bay and the Labrador Sea (not
352   shown). The CICE-simulated dynamical thickening in the Barents and Kara seas is more
353   anomalous than seen during previous CS2 years [**Figure 6**], and likely reflects the influence
354   of the positive Arctic Oscillation (AO) on ice motion [**Figure 8**]. The AO was positive from
355   December through March, a pattern which results in offshore ice advection from Siberia and
356   enhanced ice advection through Fram Strait [*Rigor et al*., 2002]. This pattern leads to
357   development of thin ice in newly formed open water areas, increasing thermodynamic ice
358   growth in the Laptev Sea, whereas increased ice advection from thick ice regions north of
359   Greenland towards Fram Strait, combined with changes in internal ice stress as the ice cover
360   has thinned, leads to more deformation. Interestingly, while the CICE model runs confirm
361   overall slightly thinner ice within the Barents Sea in April 2016, consistent with the studies
362   by *Ricker et al.* [2017a] and *Boisvert et al.* [2016], the thinning from reduced thermodynamic
363   ice growth was largely offset by thickening from dynamical effects [**Figures 5 and 6**].

364

365   *Negative feedbacks*
366   Ice growth after the September minima is a result of turbulent heat flux exchanges
367   between the relatively warm ocean mixed layer and the cold autumn and winter air through
368   the snow-covered sea ice. Progressively, as the ice grows to about 1.5 to 2 m thick, the ocean
369   becomes well insulated from the atmosphere and ice growth is slowed. Thus, it is not
370   surprising that we see less thermodynamic ice growth in regions of relatively thick (> 2.5 m)
371   November ice. A case in point is seen in winter 2013/2014 when thermodynamic ice growth
372   was reduced by 9 to 10 cm, despite an overall colder winter.
373   On the other hand, thinner ice regions generally exhibit more vigorous ice growth. For
374   example, during winter 2012/2013, CICE-free, and to a lesser extent CICE-ini simulated
375   thermodynamic ice growth increased throughout much of the Arctic Ocean in areas where the
376   ice retreated in September 2012 [**Figure 6**] and where the November 2012 thickness
377   anomalies were negative [**Figure 3**]. This process of rapid winter ice growth over thin ice
378   regions represents a negative feedback, allowing for ice to form quickly over large parts of
379   the Arctic Ocean following summers with reduced ice cover and thinner November ice.
380   Thus, while summer sea ice is rapidly declining, several studies have indicated negative
381   feedbacks over winter continue to dominate [e.g. *Notz and Marotzke*, 2012; *Stroeve and Notz*,
382   2015], allowing for recovery following summers with anomalously low sea ice extent, such
383   as those observed in 2007 and 2012. This is further supported in the CICE-free simulations
384   which show the least amount of winter ice growth in 1989, and peak ice growth following the
385   2007 and 2012 record minimum sea ice extent [**Figure 9**]. As a result, mean ice growth from
386   November to April in CICE simulations from 1985 to 2017 shows a positive trend that is
387   weakly correlated to winter air temperatures or FDDs (*R=0.49*). On the other hand, we find a
388   strong inverse correlation (*R=-0.82*) between November sea ice thickness and winter ice
389   growth. Thus, because thin ice grows faster than thick ice, there is an overall stabilizing
390   effect that suggests as long as air temperatures remain below freezing, even if they are
391   anomalously warm, the ice can recover during winter. This stabilizing feedback over winter
392   means that major departures of the September sea ice extent from the long-term trend caused
393   by summer atmospheric variability generally does not persist for more than a few years
394   [*Serreze and Stroeve*, 2015].
395   However, since 2012, overall ice growth has declined as winter air temperatures have
396   increased further. The correlation from 1985 to 2012 is smaller than over the full record

The Cryosphere
Discussions

397 (*R=0.34*), suggesting a growing influence of warmer winter air temperatures though the
398 difference in correlation is not statistically significant. While there remains a large amount of
399 inter-annual variability in winter warming events, *Graham et al.* [2017] suggest a positive
400 trend in not only the maximum temperature of these warming events, but also in their
401 duration. Interestingly, there is a modest correlation between detrended FDDs and the winter
402 maxima sea ice extent (*R=0.30*); not removing the trend results in a correlation of *R=0.83*.
403 Thus, recent reductions in overall FDDs may have played a role in the last three years of
404 record low maxima extents.
405
406 **Discussion**
407 　　The CICE-simulations and CS2 thickness retrievals from CPOM and AWI show
408 consistency that the Arctic sea ice cover in April 2017 was on average 13 cm thinner than the
409 2011-2017 mean. However, it was likely not the thinnest during the CS2 data record.
410 Thickness retrievals from the different CS2 data sets showed April 2013 thickness anomalies
411 were mostly larger than in 2016, ranging from -13 to -25 cm, whereas the CICE simulations
412 showed much smaller anomalies (-3 to -12 cm). While we expect retrievals from satellite to
413 be more accurate than those from model simulations, whether or not a year is anomalously
414 low relative to another year will depend in part on the inter-annual variability in the snow
415 cover. All three CS2 products rely on the *W99* snow depth climatology. However,
416 precipitation varies considerably from one year to the next. In the CICE-free simulations,
417 snow depth is modeled using precipitation from NCEP-2. Inter-annual variability from April
418 2011 to April 2017 (calculated as standard deviation between the 7 monthly April means) is
419 shown in **Figure 10**. North of the CAA, standard deviations in snow depth are on the order of
420 12 to 14 cm, whereas other regions are on the order of 2 to 12 cm. From the *W99*
421 climatology, inter-annual variability in snow depth during the winter months was estimated to
422 be only 4 to 6 cm, significantly less than what is exhibited here. Since ice thickness increases
423 approximately 5 to 6 times the snow depth uncertainty, a 12 to 14 cm uncertainty would lead
424 to 72 to 83 cm increase in CS2-derived ice thickness. If we average for the area shown in
425 Figure 1(d), snow depth anomalies ranged from -6 cm to +6 cm, with a corresponding impact
426 of -41 to +41 cm on thickness.
427 　　Besides not accounting for inter-annual variability in snow depth, which makes assessing
428 thickness anomalies from one year to the next less certain, differences in waveform
429 processing between the three different CS2 products adds further uncertainty. The fact that
430 the NASA CS2 product is a general outlier compared to the AWI and CPOM products is
431 further highlighted in **Figure 11**. Across the area considered (e.g. areas in color shown in
432 Figure 1(c)), the difference between April and the previous November ice thickness is shown
433 for each CryoSat-2 year. The AWI and CPOM products tend to exhibit positive ice growth
434 over winter, focused north of Greenland and the CAA and sometimes also across the pole.
435 The NASA product on the other hand generally shows less ice growth between November
436 and April in most years, and even no ice growth in some regions. The reasons for this are
437 unclear, yet interestingly in winter 2016/2017, all three products show more agreement in
438 regards to thickness decreases that span a broad region north of Greenland and the CAA,
439 combined with positive increases south of the pole towards the East Siberian and Laptev seas.
440 　　Finally, how important were the April thickness anomalies in the evolution of the summer
441 ice cover in summer 2017? Several studies have discussed how thin winter ice may
442 precondition the Arctic for less sea ice at the end of the melt season as thinner ice melts and
443 open water areas form more readily in summer, enhancing the ice albedo feedback [e.g.
444 *Stroeve et al.*, 2012; *Perovich et al.*, 2008], and sea ice thickness has been used as a predictor
445 for the September sea ice extent [*Kimura et al.,* 2013]. Thus, we may have expected 2017 to
446 be among the lowest recorded sea ice extents as the ice cover was likely thinner than average

447 and the winter extent was the lowest in the satellite record. Nevertheless, the minimum extent
448 ended up as the 8th lowest in the satellite data record. This highlights the continuing
449 importance of summer weather patterns in driving the September minimum. Spring and
450 summer 2017 were dominated by several cold core cyclones, leading to near average air
451 temperatures and ice divergence [see http://nsidc.org/arcticseaicenews/ for a discussion of
452 this summer's weather patterns]. Overall, the correlation between detrended winter sea ice
453 thickness anomalies and September sea ice extent remains low [*Stroeve and Notz*, 2015].
454 Other factors such as melt pond formation in spring [*Schröder et al.*, 2014] and summer
455 weather patterns still largely govern the evolution of the summer ice pack at current thickness
456 levels [e.g. *Holland and Stroeve*, 2011]. Interestingly, predictions of the monthly mean
457 September 2017 sea ice extent based on spring melt pond fraction in May gave a value of 5.0
458 $\pm$ 0.5 million km^2, whereas the observed value was 4.80 million km^2 [See arcus.org/sipn/sea-
459 ice-outlook/2017/june].
460
461 **Conclusions**
462 In this study we examined sea ice thickness anomalies derived from three different CS2
463 data products and that simulated using CICE. Overall freezing degree days were much
464 reduced in winter 2016/2017, and subsequent sea ice thickness estimates from CryoSat-2 in
465 April 2017 suggest the ice was thinner over large parts of the Arctic Ocean. These results are
466 complimented with CICE model simulations, both with and without initializing with
467 November ice thickness distributions. While CICE simulations suggest the mean thickness
468 within the Arctic Basin in April 2017 was the thinnest over the CryoSat-2 data record,
469 corresponding CS2-derived sea ice thickness from the three different data providers put this
470 into question. However, the use of CS2-derived freeboards with a snow depth climatology
471 remains problematic because it fails to capture inter-annual snow accumulation variability
472 which remains a large source of error in current CS2 thickness retrievals. Differences in
473 processing of the radar waveform, values of snow and ice density, delineation of first-year vs.
474 multiyear ice, and sea surface height retrieval also contribute to differences among available
475 data sets, making it challenging to robustly assess inter-annual variability of ice thickness
476 from CryoSat-2. Despite these challenges it is encouraging that in most years, the interannual
477 variability in positive and negative anomalies is consistent between the 3 CS2 data sets.
478 Finally, CICE-free simulations from 1985 to 2017 reveal the correlation between winter
479 ice growth and November ice thickness ($R=-0.82$) is stronger than between growth and FDDs
480 ($R=0.49$), highlighting the importance of the negative winter growth feedback mechanism.
481 This supports previous studies that the long-term sea ice reduction in the Arctic Basin is
482 mainly driven by summer atmospheric conditions. However, this correlation has become
483 weaker since 2012, indicating that higher winter air temperatures and further delays in
484 autumn/winter freeze-up due to warmer mixed-layer ocean temperatures prohibit a complete
485 recovery of winter ice thickness in spite of the negative feedback mechanism. This is
486 highlighted by the fact that overall thermodynamic ice growth for winter 2016/2017 was just
487 under 1m despite 2016 reaching the second lowest minimum extent recorded during the
488 satellite record.
489
490 **Acknowledgements**

497 2013-04). NASA CryoSat-2 data provided courtesy of Nathan Kurtz. NCEP2 data obtained
498 from NOAA Earth System Research Laboratory
499 (http://www.esrl.noaa.gov/psd/data/gridded/data.ncep.reanalysis2.gaussian.html).
500 Data policy: data available upon request.
501

References

503 Armitage, T. W., and A.L. Ridout, (2015), Arctic sea ice freeboard from AltiKa and
504   comparison with CryoSat-2 and Operation IceBridge. *Geophys. Res. Lett.*, *42*(16), 6724-
505   6731, doi:10.1002/2015GL064823.
506 Bekryaev, R.V., I.V. Polyakov and V.A. Alexeev (2010), Role of polar amplification in long-
507   term surface air temperature variations and modern Arctic warming, *J. Clim*, 23, 3888-
508   3906.
509 Bitz, C.M. and G.H. Roe (2004), A mechanism for the high rate of sea ice thinning in the
510   Arctic Ocean, *J. Clim*. 17, 2623-2632, doi:10.1175/1520-
511   0442(2004)017<3623:AMFTHR>2.0CO;2.
512 Boisvert, L.N., A.A. Petty, and J. Stroeve (2016), The Impact of the Extreme Winter 2015/16
513   Arctic Cyclone on the Barents–Kara Seas, *Bull. Amer. Met. Soc.*, doi:10.1175/MWR-D-16-
514   0234.1.
515 Cohen, L., S. R. Hudson, V. P. Walden, R. M. Graham, M. A. Granskog (2017), Meteorological
516   conditions in a thinner Arctic sea ice regime from winter through early summer during
517   the 388 Norwegian young sea ICE expedition (N-ICE2015), *J. Geophys. Res. Atmos.*,
518   doi:10.1002/2016JD026034.
519 Cullather, R. I., Y. Lim, L. N. Boisvert, L. Brucker, J. N. Lee, and S. M. J. Nowicki (2016),
520   Analysis of the 426 warmest Arctic winter, 2015-2016, *Geophys. Res. Lett.*, 808–816,
521   doi:10.1002/2016GL071228.
522 Dee, D. P. et al. (2011), The ERA-Interim reanalysis: Configuration and performance of the
523   data 428 assimilation system, *Q. J. R. Meteorol. Soc.*, 137(656), 553–597,
524   doi:10.1002/qj.828.
525 Flocco, D., D. Schröder, D. L. Feltham, and E. C. Hunke (2012), Impact of melt ponds on
526   Arctic sea ice simulations from 1990 to 2007, *J. Geophys. Res.*,
527   doi:10.1029/2012JC008195.
528 Graham, R.M., L. Cohen, A.A. Petty, L.N. Boisvert, A. Rinke, S.R. Hudson, M. Nicolaus and
529   M.A. Granskog, (2017), increasing frequency and duration of Arctic winter warming
530   events, *Geophys. Res. Lett.*,
531 Graversen, R.G. and M. Burtu (2016), Arctic amplification enhanced by latent energy
532   transport of atmospheric planetary waves, *Quart. Royal Meteoro. Soc.*,
533   doi:10.1002/qj.2802.
534 Graversen RG. (2006), Do changes in midlatitude circulation have any impact on the Arctic
535   surface air temperature trend? *J. Clim*. **19**: 5422–5438.
536 Hendricks, S., R. Ricker and V. Helm (2016), User Guide – AWI CryoSat-2 sea ice thickness
537   data product (V1.2).
538 Holland, M.M. and J.C. Stroeve (2011), Changing seasonal sea ice predictor relationships in a
539   changing Arctic climate, Geophys. Res. Lett., doi:10.1029/2011GL049303.
540 Hunke, E. C., W. H. Lipscomb, A. K. Turner, N. Jeffery, and S. Elliott (2015), CICE: the Los
541   Alamos Sea Ice Model Documentation and Software User's Manual Version 5.1.

542   Jakobshavn, E., T. Vihma, T. Palo, L. Jakobson, H. Keernik and J. Jaagus (2012), validation of
543   atmospheric reanalysis over the central Arctic Ocean, *Geophys. Res. Lett*., 39, L10802,
544   doi:10.1029/2012GL051591.
545   Kanamitsu, M., W. Ebisuzaki, J. Woollen, S-K Yang, J.J. Hnilo, M. Fiorino, and G. L. Potter
546   (2002, updated 2017), NCEP-DOE AMIP-II Reanalysis (R-2): 1631-1643, *Bull. Amer. Met.*
547   *Soc*.
548   Kimura, N., A. Nishimura, Y. Tanaka and H. Yamaguchi (2013), Influence of winter sea-ice
549   motion on summer ice cover in the Arctic, *Polar Research*, 32,
550   doi:10.3402/polar.v32i0.20193.
551   Kurtz, N. and J. Harbeck. 2017. *CryoSat-2 Level 4 Sea Ice Elevation, Freeboard, and Thickness,*
552   *Version 1*. [Indicate subset used]. Boulder, Colorado USA. NASA National Snow and Ice
553   Data Center Distributed Active Archive Center. [Date Accessed].
554   Kurtz, N.T., N. Galin and M. Studinger (2014), An improved CryoSat-2 sea ice freeboard
555   retrieval algorithm through the use of a waveform fitting, The Cryosphere, 8, 1217-1237,
556   doi:10.5194/tc-802017-2014.
557   Laxon, S. W., K.A. Giles, A.L. Ridout, D.J. Wingham, R. Willatt, R. Cullen, R. Kwok, A.
558   Schweiger, J. Zhang, C. Haas, S. Hendricks, R. Krishfield, N. Kurtz, S. Farrell, and M.
559   Davidson, (2013), CryoSat-2 estimates of Arctic sea ice thickness and volume, *Geophys.*
560   *Res. Lett*., 40, 732–737, doi:10.1002/grl.50193.
561   Laxon, S. W., K. A. Giles, A. L. Ridout, D. J. Wingham, R. Willatt, R. Cullen, R. Kwok, 393 A.
562   Schweiger, J. Zhang, C. Haas, S. Hendricks, R. Krishfield, N. Kurtz, S. Farrell, 394 and M.
563   Davidson (2013), Cryosat-2 estimates of arctic sea ice thickness and volume, 395
564   *Geophys. Res. Lett*, 40 (4), 732–737, doi:10.1002/grl.50193.
565   Merkouriadi, I., B. Cheng, R.M. Graham, A. Rosel and M.A. Granskog (2017), Critical role of
566   snow on sea ice growth in the Atlantic sector of the Arctic Ocean, *Geophysical Research*
567   *Letters*, 44, 10-479-10,485, doi:10.1002/2017GL075494.
568   Moore, G. W. K. (2016), The December 2015 North Pole Warming Event and the Increasing
569   457 Occurrence of Such Events, *Sci. Rep*., 6(November), 39084, doi:10.1038/srep39084.
570   Notz, D. and J. Marotzke (2012), Observations reveal external driver for Arctic sea ice
571   retreat, *Geophys. Res. Lett*., doi:10.1029/2012GL051094.
572   Overland, J. E., and M. Wang (2016), Recent extreme arctic temperatures are due to a split
573   polar vortex, *J. Clim*., 29(15), 5609–5616, doi:10.1175/JCLI-D-16- 0320.1.
574   Perovich, D.K., J.A. Richter-Menge, K.F. Jones and B. Light (2008), Sunlight, water and ice:
575   Extreme Arctic sea ice melt during the summer of 2007, *Geophys. Res. Lett*.,
576   doi:10.1029/2008GL034007.
577   Pithan, F. and T. Mauritsen (2014), Arctic amplification dominated by temperature
578   feedbacks in contemporary climate models, *Nature Geoscience*, 7, 181-184,
579   doi:10.1038/ngeo2017.
580   Polyakov I.V., A. Beszczynska, E.C. Carmack, I.A. Dmitrenko, E. Fahrbach, I.E. Frolov, R.
581   Gerdes, E. Hansen, J. Holfort, V.V. Ivanov, M.A. Johnson, M. Karcher, F. Kauker, J.
582   Morison, K.A. Orvik, U. Schauer, H.L. Simmons, A. Skagseth, V.T. Sokolov, M. Steele, L.A.
583   Timokhov, D. Walsh and J.E. Walsh (2005), One more step towards a warmer
584   Arctic. *Geophys. Res. Lett*. 32, L17605, doi: 10.1029/2005GL023740.
585   Rae, J.G.L., H.T. Hewitt, A.B. Keen, J.K. Ridley, J.M. Edwards, and C.M. Harris (2014), A
586   sensitivity study of the sea ice simulation in HadGEM3, *Ocean Model*. 74, 60–76,
587   doi:10.1016/j.ocemod.2013.12.003.

588 Ricker, R., S. Hendricks, F. Girard-Ardhuin, L. Kaleschke, C. Lique, X. Tian-Kunze, M. Nicolaus,
589   and T. Krumpen (2017a), Satellite observed drop of Arctic sea ice growth in winter 2015-
590   2015, *Geophys. Res. Lett.*, doi:10.1002/2016GL072244.
591 Ricker, R., S. Hendricks, L. Kaleschke, X. Tian-Kunze, J. King and C. Haas (2017b), A weekly
592   arctic sea-ice thickness data record from merged cryosat-2 and SMOS satellite data, *The
593   Cryosphere*, 1-27, doi:10.5194/tc-2017-4.
594 Ricker, R., S. Hendricks, V. Helm, H. Skourup, and M. Davidson (2014a), Sensitivity of
595   CryoSat-2 Arctic sea-ice freeboard and thickness on radar-waveform interpretation, *The
596   Cryosphere*, 8 (4), 1607-1622, doi:10.5194/tc-8-1607-2014.
597 Rigor, I.G., J.M. Wallace and R.L. Colony (2002), Response of sea ice to the Arctic Oscillation,
598   *J. Clim.*, doi:10.1175/1520-0442(2002)015<2648:ROSITT>2.0.CO;2.
599 Schröder D., D. L. Feltham, D. Flocco, M. Tsamados (2014), September Arctic sea-ice
600   minimum predicted by spring melt-pond fraction. *Nature Clim. Change*, doi
601   10.1038/NCLIMATE2203.
602 Screen, J.A and I. Simmonds (2010), The central role of diminishing sea ice in recent Arctic
603   temperature amplification, *Nature*, 464, 1334-1337.
604 Serreze, M.C., A.P. Barrett, J.C. Stroeve, D.M. Kindig, M.M. Holland (2009), The emergence
605   of surface-based Arctic amplification, *The Cryosphere*, 3, pp. 11–19.
606 Stroeve, J. and D. Notz (2015), Insights on past and future sea-ice evolution from combining
607   observations and models, *Global and Planetary Change*,
608   doi:10.1016/gloplacha.2015.10.011.
609 Stroeve, J.C., T. Markus, L. Boisvert, J. Miller and A. Barrett (2014), Changes in Arctic Melt
610   Season and Implications for Sea Ice Loss. Geophysical Research Letters,
611   doi:10.1002/2013GL058951.
612 Stroeve, J.C., M.C. Serreze, J.E. Kay, M.M. Holland, W.N. Meier and A.P. Barrett, (2012). The
613   Arctic's rapidly shrinking sea ice cover: A research synthesis, *Clim. Change*, doi:
614   10.1007/s10584-011-0101-1.
615 Tilling, R. L., A. Ridout, A. Shepherd, and D. J. Wingham (2015), Increased arctic sea 454 ice
616   volume after anomalously low melting in 2013, *Nature Geoscience*, 8 (8), 643–646.
617 Tilling, R. L., A. Ridout and A. Shepherd (2016), Tilling, R. L., A. Ridout, and A. Shepherd,
618   Near-real-time Arctic sea ice thickness and volume from CryoSat-2, *The Cryosphere*, 10,
619   doi:10.5194/tc-10-2003-2016.
620 Tilling, R.L., A. Ridout, and A. Shepherd (2017), Estimating Arctic sea ice thickness and
621   volume using CryoSat-2 radar altimeter data, *Advances in Space Research*,
622   doi:10.1016/j.asr.2017.10.051.
623 Tsamados M., D. L. Feltham, D. Schröder, D. Flocco, S. Farrell, N. Kurtz, S.Laxon, and S. Bacon
624   (2014), Impact of variable atmospheric and oceanic form drag on simulations of Arctic
625   sea ice. *J. Phys. Oceanogr*. 44 (1329-1353), doi:10.1175/JPO-D-13-0215.1.
626 Tsamados, M., D. Feltham, A. Petty, D. Schröder and D. Flocco (2015), Processes controlling
627   surface, bottom and lateral melt of Arctic sea ice in a state of the art sea ice model, *Phil.
628   Trans. R. Soc. A* 373.2052, doi:10.1098/rsta.2014.0167.
629 Warren, S.G., I.G. Rigor, N. Untersteiner, V.F. Radionov, N.N. Bryazgin, Y.I. Aleksandrov and
630   R. Barry (1999), Snow depth on Arctic sea ice, J. Clim., 12, 1814-1829.
631 Willatt, R., S. Laxon, K. Giles, R. Cullen, C. Haas, and V. Helm (2011), Ku-band radar
632   penetration into snow cover Arctic sea ice using airborne data, *Ann. Glaciol.*, **52**(57), 197–
633   205.
634

The Cryosphere
Discussions

Open Access

EGU

638   **Table 1**. Regional trends in freeze-up, 2017 freeze-up date and anomaly (relative to 1981-
639   2010 mean).

Region	Freeze-up Trend (days per decade)	2017 Mean Freeze-up (day of year)	2017 Freeze-up Anomaly (days)
Sea of Okhotsk	9.1	304	0.8
Bering Sea	6.7	338	25.2
Hudson Bay	7.9	333	16.9
Baffin Bay	8.0	312	13.2
E. Greenland Sea	5.6	267	2.7
Barents Sea	13.6	347	60.3
Kara Sea	10.7	314	36.6
Laptev Sea	9.0	272	10.7
E. Siberian Sea	11.8	286	27.1
Chukchi Sea	14.1	314	31.0
Beaufort Sea	8.9	279	23.4
Canadian Archipelago	4.9	268	12.7
Central Arctic	3.1	255	16.8
Pan-Arctic	7.5	288	19.6

640
641   **Table 2.** Mean November ice thickness and anomaly with respect to the 2011-2017 mean (in
642   parenthesis) from CS2 derived from CPOM, AWI and NASA. Spatial mean is over Arctic Basin,
643   defined as the area for which CS-data were available continuously for all 7 winter periods
644   November to April 2010/2011 to 2016/17. This region corresponds to all three regions
645   shown in Figure 1(c).

	November SIT CS2 CPOM (cm)	November SIT CS2 AWI (cm)	November SIT CS2 NASA (cm)	November SIT CICE-free (cm)
2010	183 (-6)	208 (-8)	198 (-7)	206 (+6)
2011	157 (-32)	174 (-42)	170 (-35)	185 (-15)
2012	173 (-16)	192 (-24)	177 (-28)	152 (-48)
2013	212 (+23)	246 (+29)	243 (+38)	208 (+08)
2014	207 (+18)	239 (+23)	226 (+21)	231 (+31)
2015	196 (+7)	229 (+13)	217 (+12)	219 (+19)
2016	193 (+4)	225 (+9)	204 (-1)	199 (-1)
2010-2016 mean	189	216	205	200

646
647

648

649

The Cryosphere
Discussions
Open Access
EGU

Table 3. Mean April sea ice thickness (SIT) and anomaly with respect to the 2011-2017 mean
(in parenthesis) from three CS2 products (CPOM, AWI and NASA), and the CICE (free run
1985-2017) and CICE runs initialized with CS2 ice thickness in November. The amount of
thermodynamic ice growth and dynamical ice change from the CICE model runs is also
given. Spatial mean is over Arctic Basin, defined as the area shown in Figure 1(d).

|	CryoSat-2 Results			CICE Simulations					
	April SIT CPOM (cm)	April SIT AWI (cm)	April SIT (NASA) (cm)	April SIT CICE free (cm)	April SIT CICE ini (cm)	Therm growth CICE free (cm)	Therm growth CICE ini (cm)	Dyn change CICE free (cm)	Dyn change CICE ini (cm)
1990-2017 Mean	n/a	n/a	n/a	283	n/a	107	n/a	-18	n/a
2010-2017 Mean	243	230	235	246	240	112	103	-15	-17
2011	239 (-4)	237 (+7)	227 (-8)	242 (-4)	241 (+1)	115 (+3)	104 (+1)	-18 (-3)	-20 (-3)
2012	235 (-8)	219 (-11)	218 (-17)	247 (+1)	233 (-7)	115 (+3)	110 (+7)	-9 (+6)	-12 (+5)
2013	230 (-13)	208 (-22)	210 (-25)	234 (-12)	237 (-3)	136 (+24)	117 (+14)	-16 (+1)	-19 (-2)
2014	261 (+18)	250 (+20)	254 (+19)	251 (+5)	249 (+9)	102 (-10)	94 (-9)	-12 (+3)	-17 (+0)
2015	264 (+21)	252 (+22)	254 (+19)	264 (+18)	255 (+11)	108 (-4)	103 (-0)	-18 (-3)	-22 (-5)
2016	239 (-4)	227 (-3)	228 (-7)	254 (+8)	241 (+1)	107 (-5)	101 (-2)	-15 (-0)	-17 (+0)
2017	230 (-13)	218 (-12)	238 (+3)	233 (-13)	227 (-13)	99 (-13)	92 (-11)	-14 (+1)	-13 (+4)
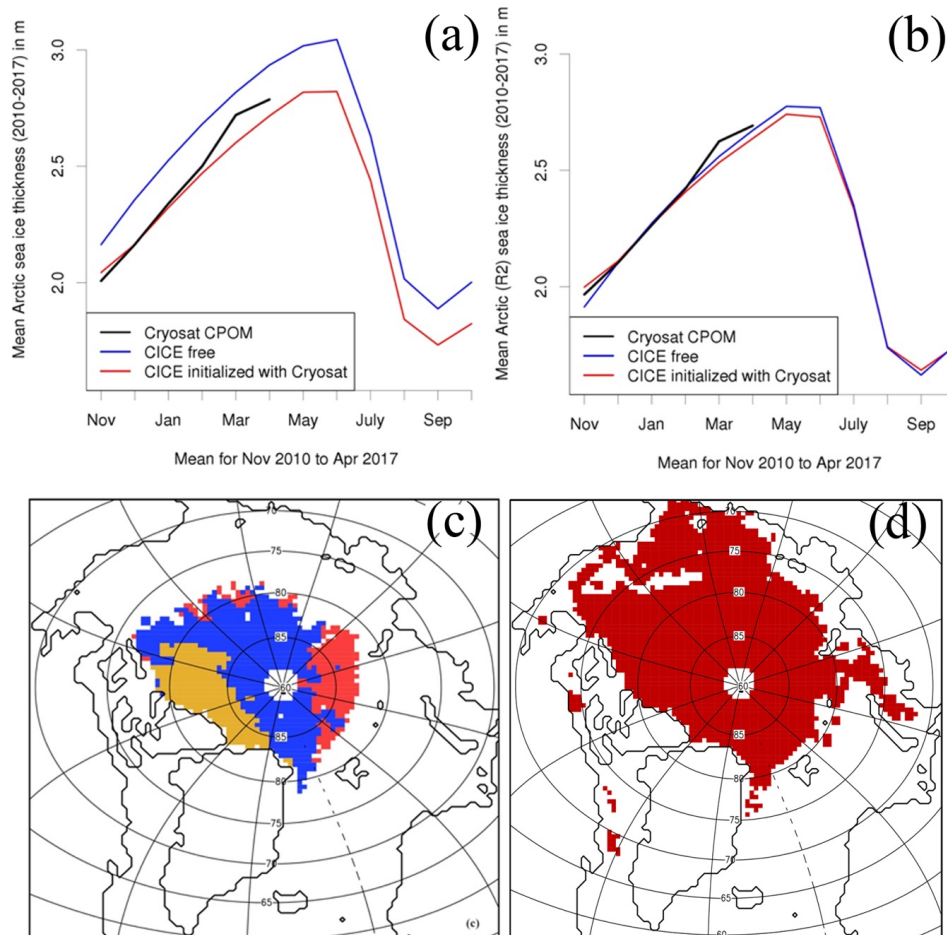
Figure 1. Comparison of CPOM CryoSat-2 mean seasonal sea ice thickness (black) with CICE free (blue) and CICE initialized with Cryosat-2 in November (red). Figure 1(a) shows results for mean thickness averaged over all the colored areas shown Figure1(c), representing the total region for which Cryosat-2 data exist in November (only grid points included with > 100 measurements per month and mean thickness > 0.5m) and (b) mean thickness averaged over the sub-region shown in blue with medium thick ice in January (between 1.5 and 2.5m). Blue areas in Figure 1(c) show regions between November and January where CryoSat-2 thickness are between 1.5 and 2.5 m in all years. Figure 1(d) is the region over which the April thickness anomalies and results are presented.
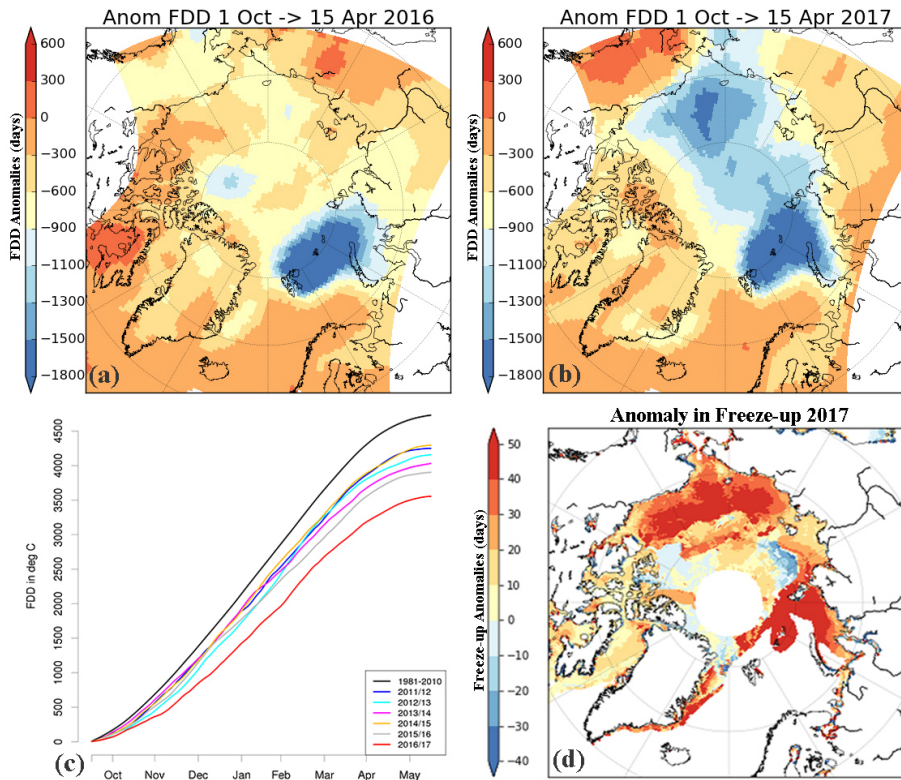
Figure 2. Top panel shows the freezing degree anomalies (FDD) computed as the number of
days with NCEP2 2m air temperature below -1.8°C from mid-November to mid-April in
winter 2016 (a) and winter 2017 (b) computed relative to the 1981-2010 climatology.
Bottom left image shows the cumulative freezing degree days (FDDs) averaged over region
shown in Figure 3 inset (c), and bottom right image shows freeze-up anomalies for
2016/2017 relative to 1981-2010 (d). Areas in white are either missing (pole hole) or no sea
ice in winter 2016/2017. Light gray areas are open ocean.
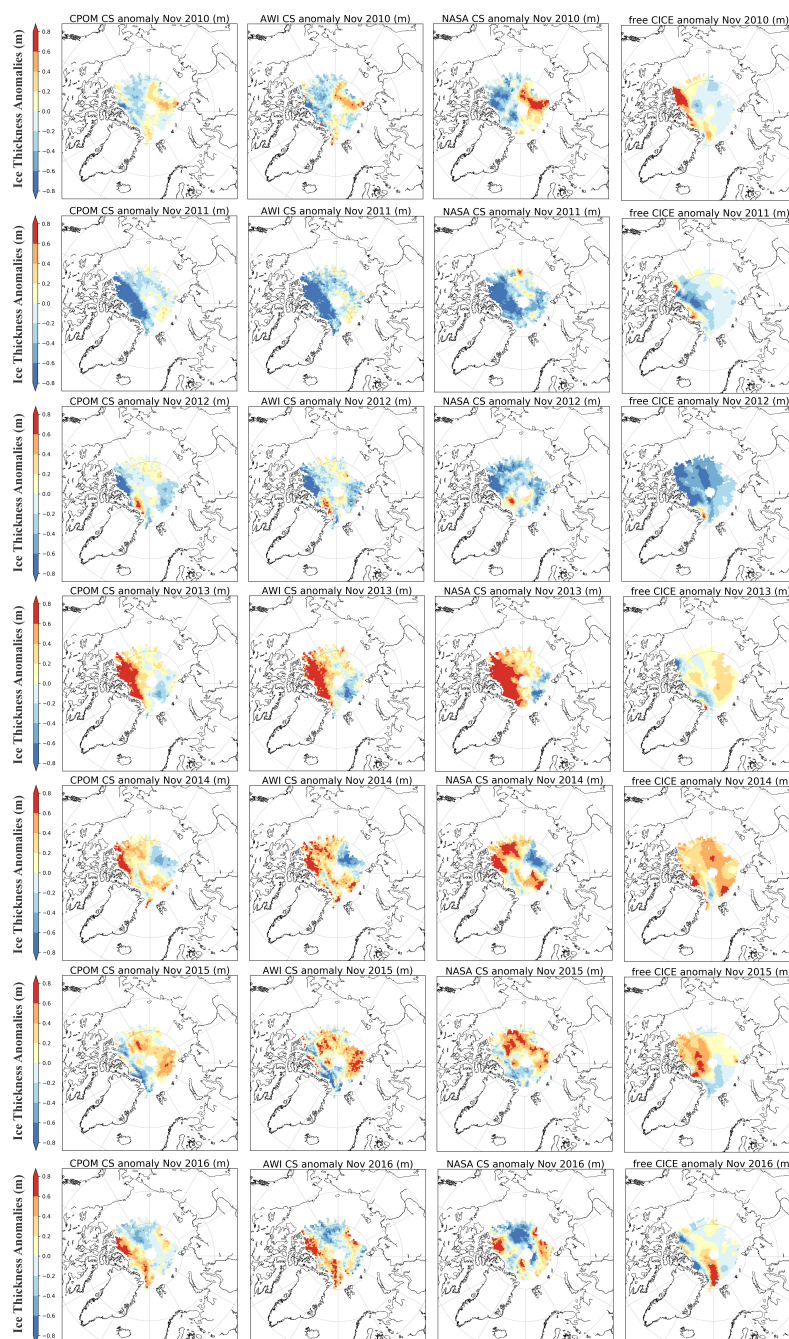
679
680   **Figure 3**. November ice thickness anomaly relative to 2010-2016 in cm based on CryoSat-2
681   data from UCL CPOM (left), Alfred Wegener Institute (AWI) (middle) and NASA (right). Grid
682   points with less than 100 individual measurements and a mean sea ice thickness of less than
683   0.5 m are not included. CICE-free thickness anomalies are also shown in the left right
684   column.

685
686
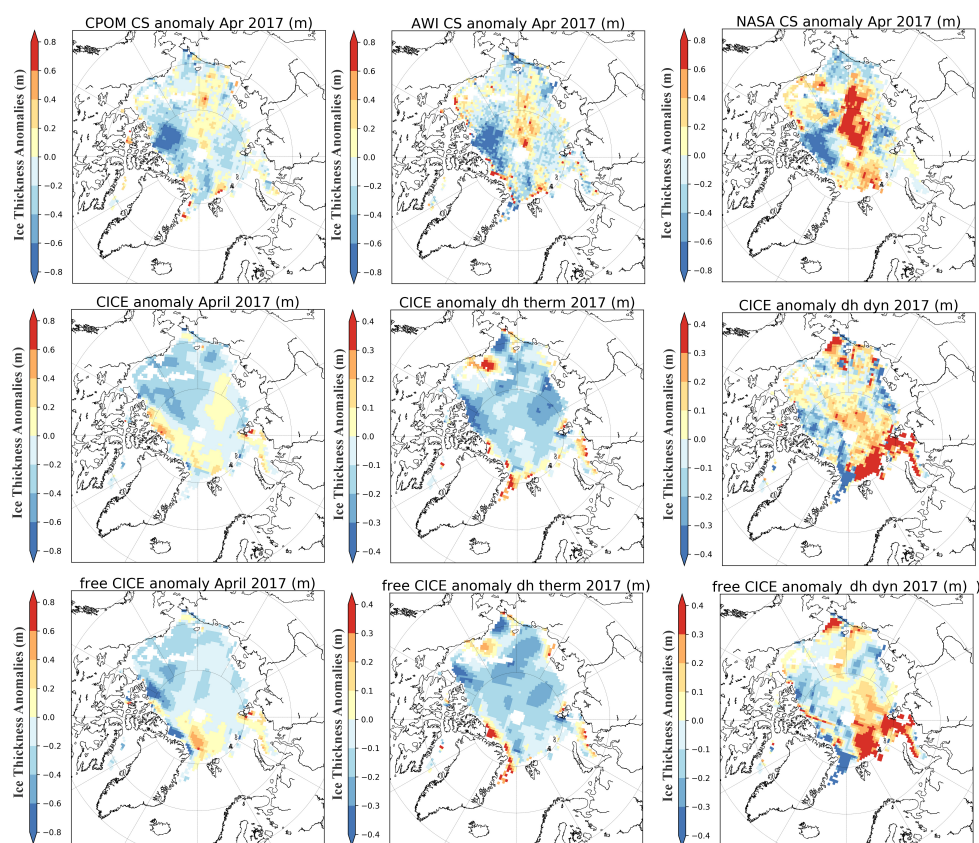
687
688 **Figure 4.** CryoSat-2 and CICE simulated thickness anomalies in April 2017 relative to the
689 2011-2017 mean. Top images show the total ice thickness anomalies from CryoSat-2 for
690 CPOM (left), AWI (middle) and NASA (right). The middle left image shows April 2017
691 thickness anomalies from CICE initialized with CPOM November CS2 thickness together with
692 the contributions from thermodynamics (middle) and dynamics (left) and bottom show the
693 corresponding results from the CICE free simulations. Grid points with less than 100
694 individual measurements and a mean sea ice thickness of less than 0.5 m are not included.
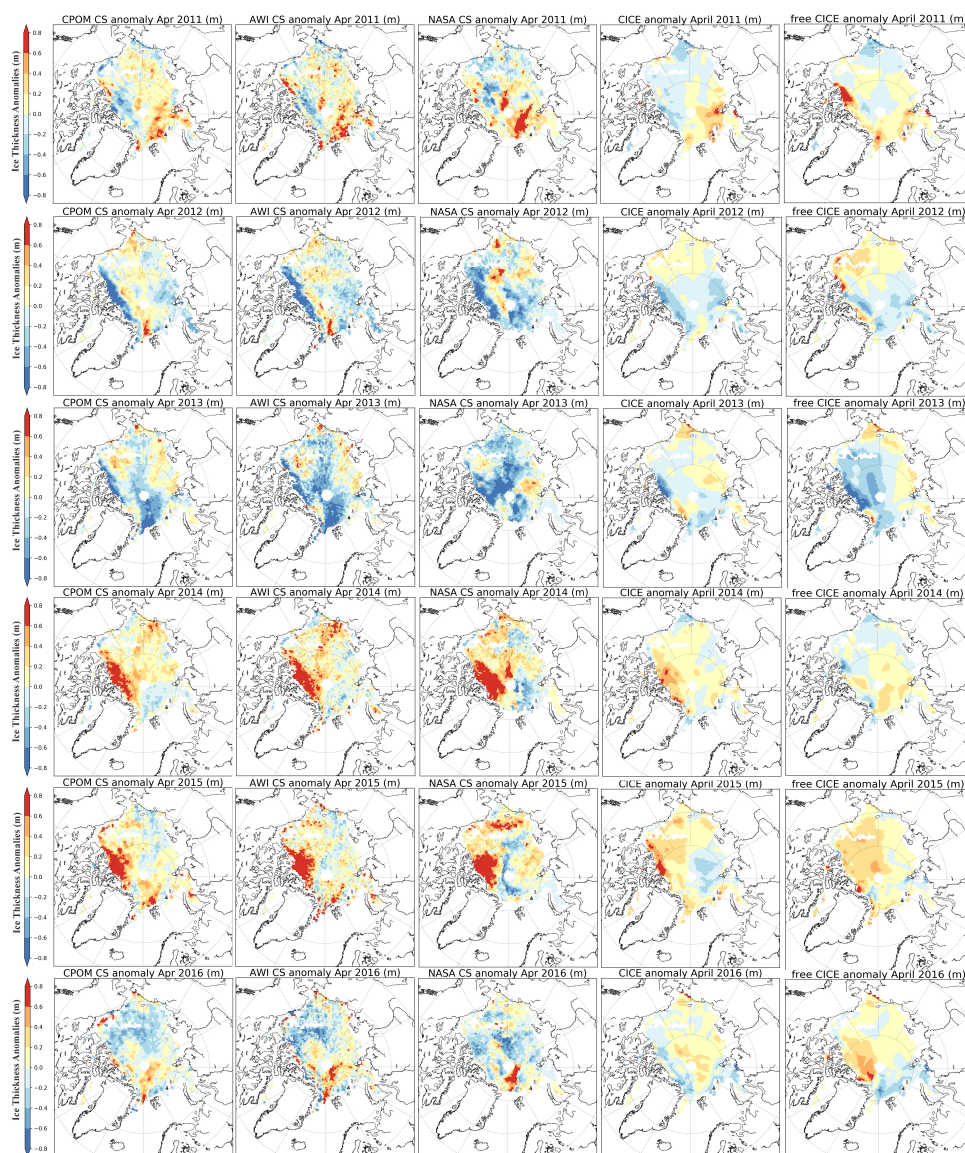
695
Figure 5. Anomaly of April ice thickness from 2011 to 2016 in m relative to the 2011 to 2017
mean from CryoSat-2 CPOM (far left), AWI (second left), NASA (middle), CICE simulations
initialized with November CPOM CryoSat-2 thickness fields (2nd right), and CICE simulations
not initialized with CryoSat-2 thickness (right). Grid points with less than 100 individual
measurements and a mean sea ice thickness of less than 0.5 m are not included.

701

The Cryosphere
Discussions
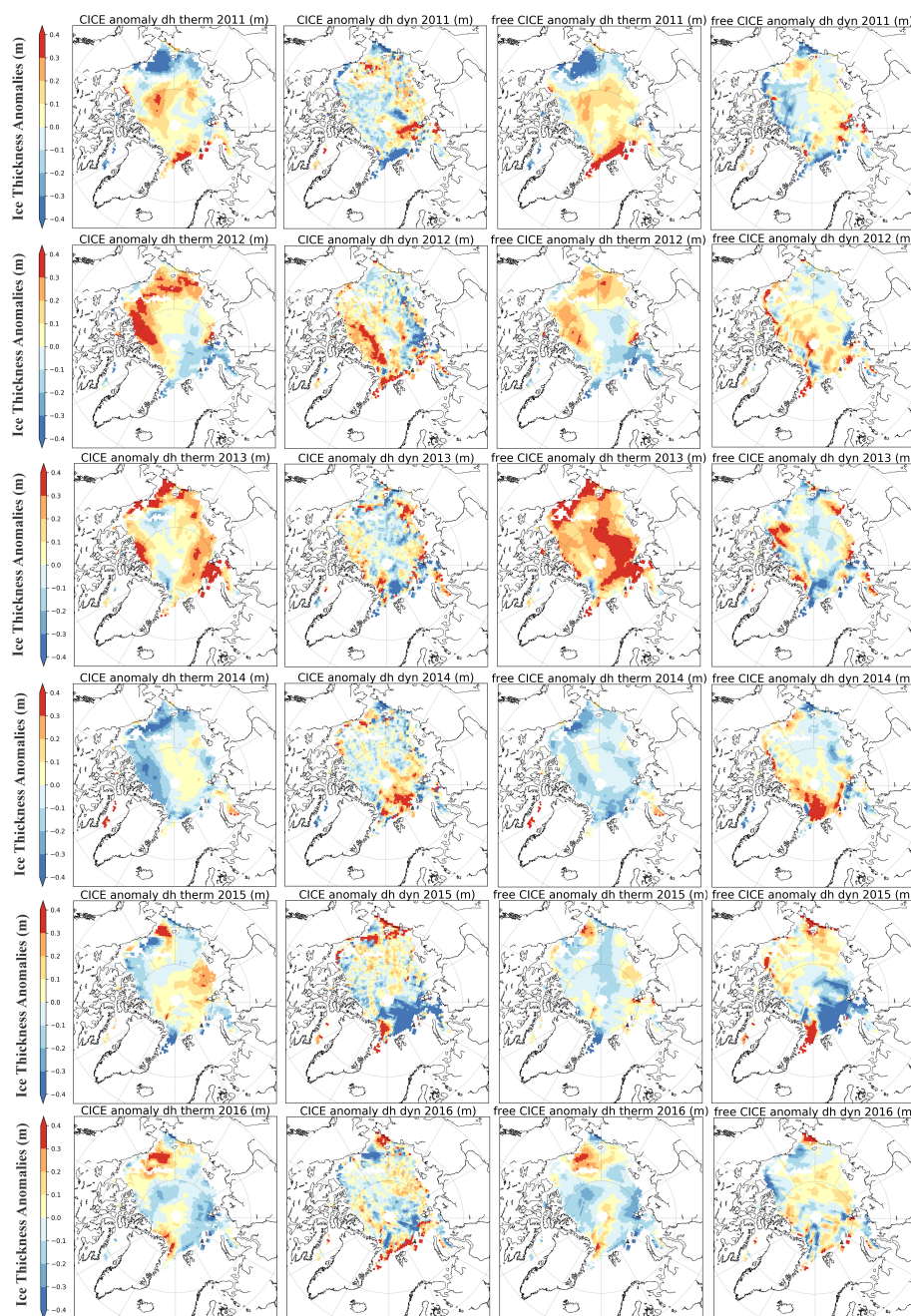
Figure 6. Anomalies of CICE simulated thermodynamic ice growth and dynamical thickness changes in m relative to the 2011 to 2017 mean from the CICE simulations initialized with November CPOM CryoSat-2 thickness fields (left), and CICE simulations not initialized with CryoSat-2 thickness (right). The year in title reflects the end month over which ice growth occurs (e.g. from November to April).
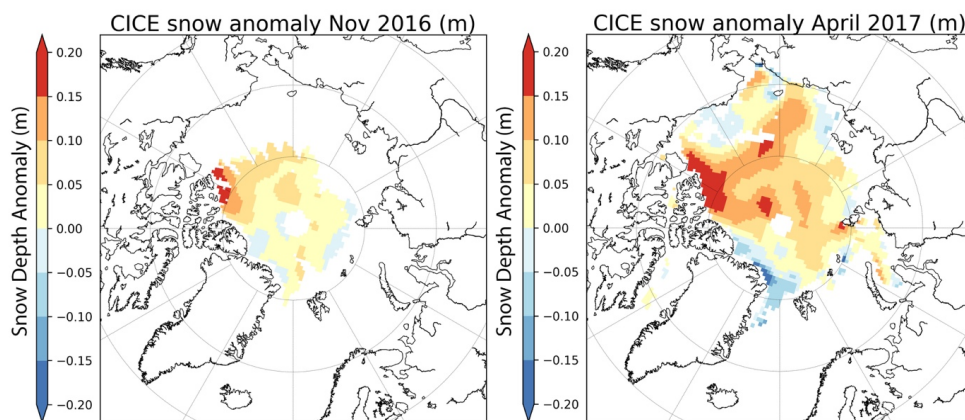
709
710 **Figure 7**. Snow depth anomaly for November 2016 (relative to 2010-2016) and April 2017
711 (relative to 2011-2017) from CICE.
712
713
714
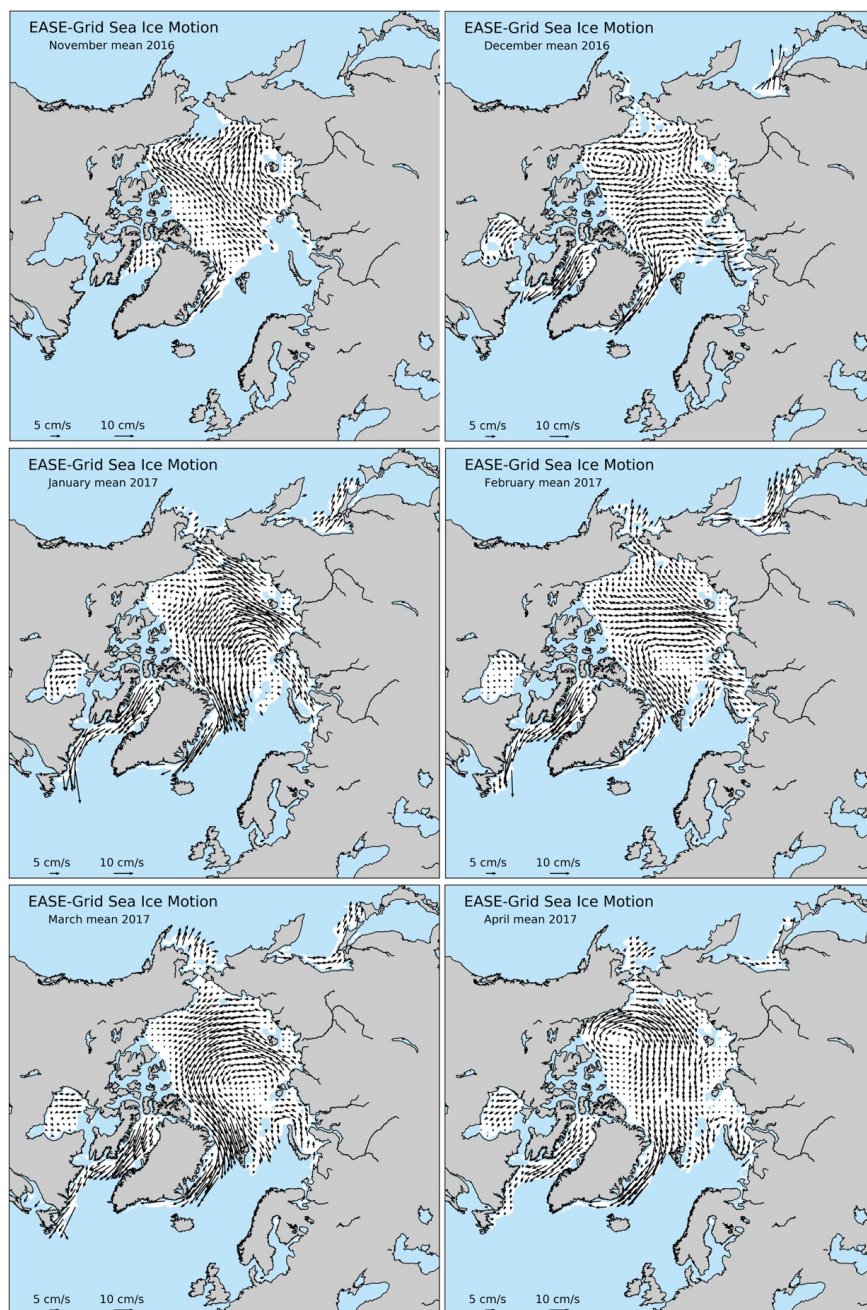
Figure 8. Mean monthly sea ice motion from the NSIDC Polar Pathfinder Data Set.
Preliminary data provided by Scott Stewart, NSIDC.
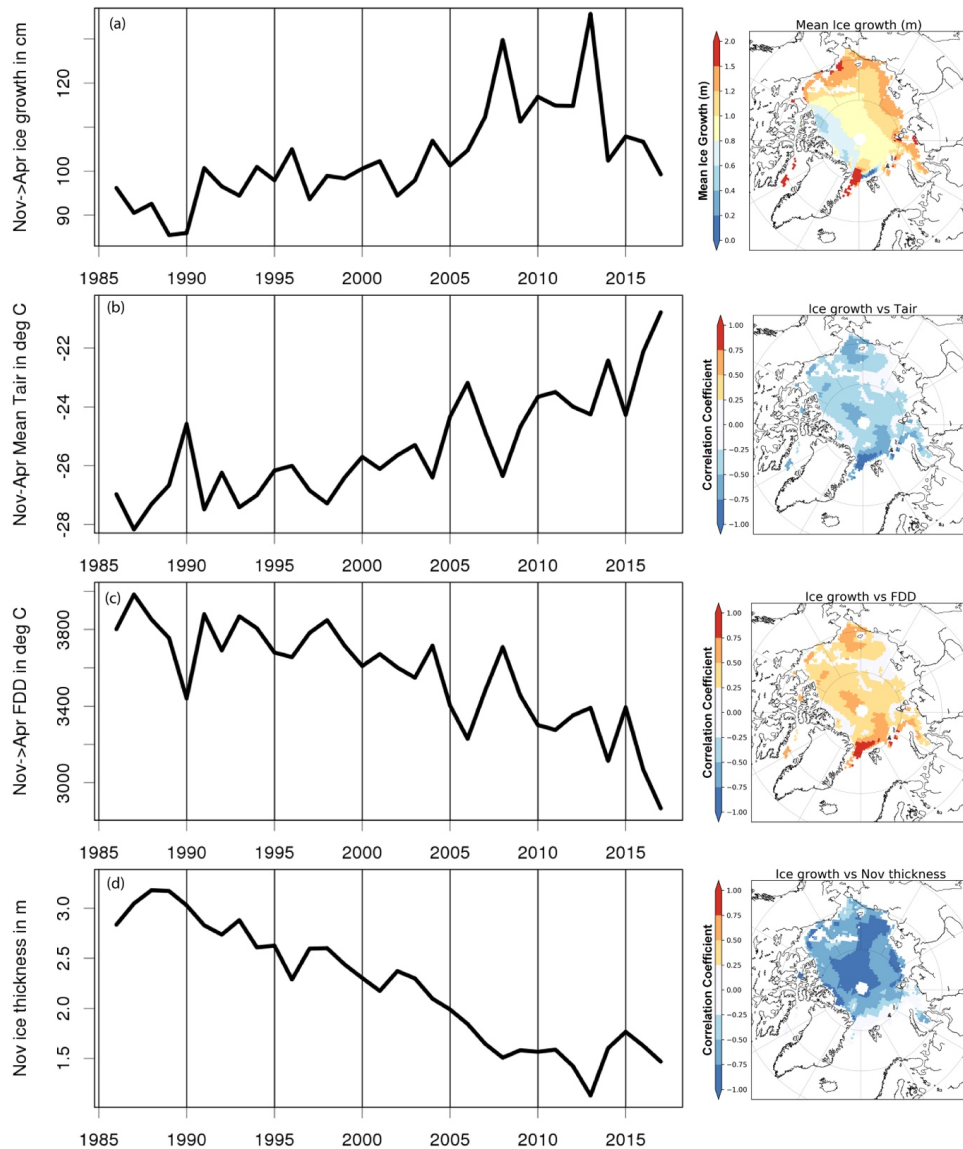
**Figure 9.** Time-series from 1985 to 2017 of mean winter ice growth (mid-November to mid-April) in the free CICE simulation (a), mean 2m NCEP-2 air temperature (b), cumulative freezing degree days (FDDs) (c) and November ice thickness (d). All time-series results are averaged over the areas shown in Figure S1(c). Corresponding images to the left of each time-series plots show: mean ice growth from November to April as averaged from 1985/1986 to 2016/2017; correlation coefficient between ice growth and 2m NCEP-2 air temperature; correlation coefficient between ice growth and FDDs; and correlation coefficient between ice growth and November ice thickness, respectively. All correlation values are given for linear regression of de-trended time series.

24
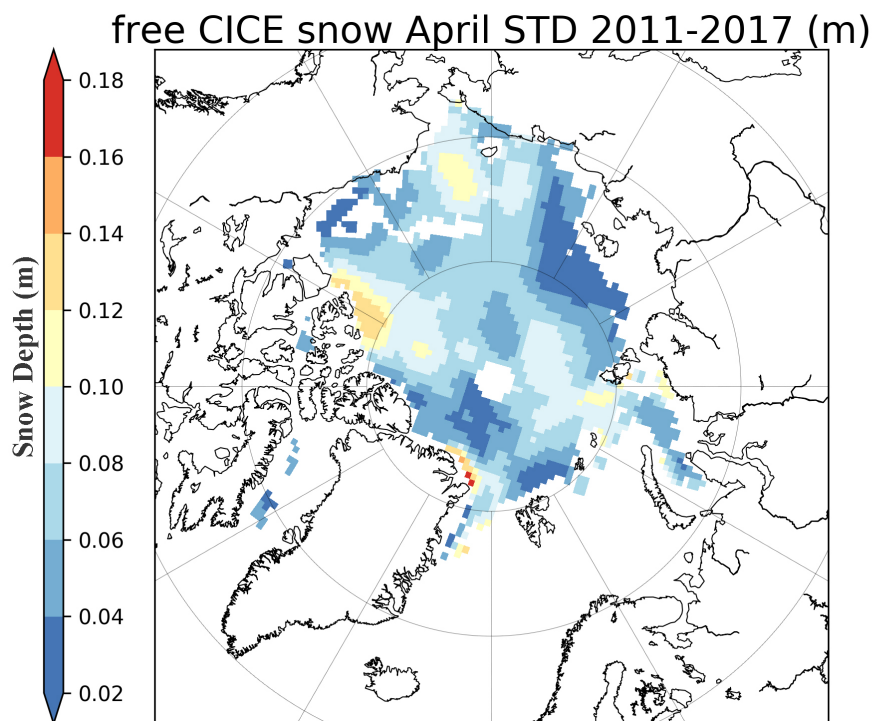
Figure 10. Standard deviation of CICE-simulated snow depth using NCEP-2 reanalysis for the month of April from 2011 to 2017.
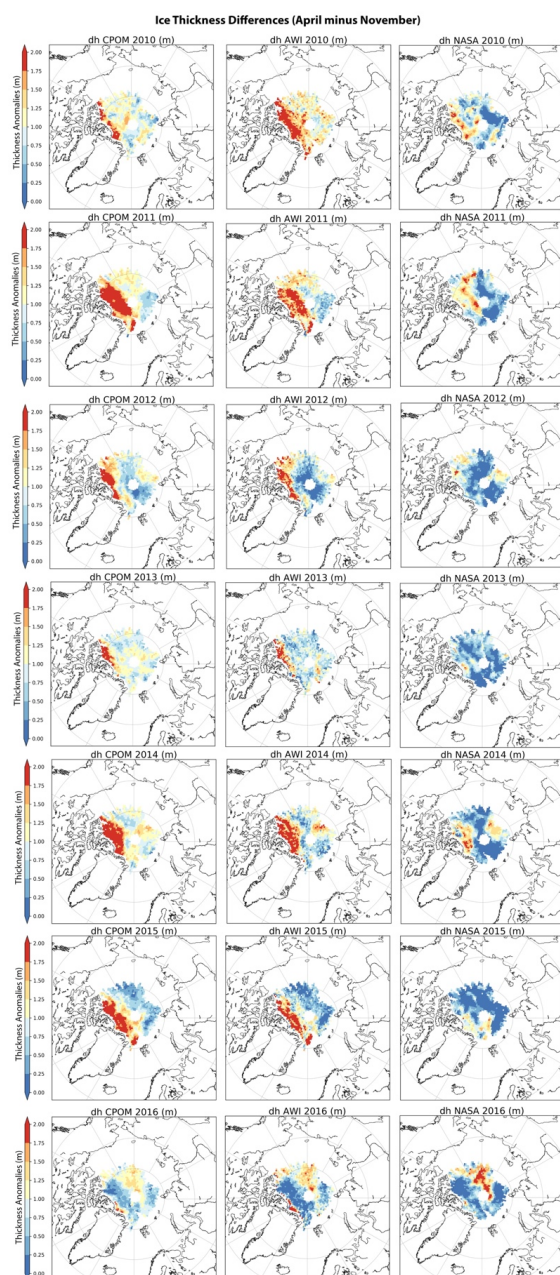
733
734 **Figure 11**. Comparison between ice growth (April minus November) in the UCL CPOM
735 CryoSat-2 thickness retrievals (left) and those from the Alfred Wegener Institute (AWI)
736 (middle) and NASA (right). The year shown corresponds to the November months, such that
737 2016 refers to ice thickness differences between April 2017 and November 2016. Results are
738 only shown for the area shown in Figure 1(c), which represents grid points that had more
739 than 100 individual measurements and a mean sea ice thickness greater than 0.5 m during
740 the November months.